

Optical Transistor for an Amplification of Radiation in a Broadband THz Domain

K. H. A. Villegas,¹ F. V. Kusmartsev,^{2,3,*} Y. Luo,² and I. G. Savenko^{1,4}

¹*Center for Theoretical Physics of Complex Systems,
Institute for Basic Science (IBS), Daejeon 34126, Korea*

²*Micro/Nano Fabrication Laboratory Microsystem and THz Research Center, Chengdu, Sichuan, China*

³*Loughborough University, UK*

⁴*A. V. Rzhanov Institute of Semiconductor Physics,
Siberian Branch of Russian Academy of Sciences, Novosibirsk 630090, Russia*

(Dated: March 3, 2020)

We propose a new type of optical transistor for a broadband amplification of THz radiation. It is made of a graphene–superconductor hybrid, where electrons and Cooper pairs couple by Coulomb forces. The transistor operates via the propagation of surface plasmons in both layers, and the origin of amplification is the quantum capacitance of graphene. It leads to THz waves amplification, the negative power absorption, and as a result, the system yields positive gain, and the hybrid acts like an optical transistor, operating with the terahertz light. It can, in principle, amplify even a whole spectrum of chaotic signals (or noise), that is required for numerous biological applications.

The growing interest in terahertz (THz) frequency range (0.3 to 30 THz) is due to its potential applications in diverse fields such as non-destructive probing in medicine, allowing for non-invasive tumor detection, biosecurity, ultra-high bandwidth wireless communication networks, vehicle control, atmospheric pollution monitoring, inter-satellite communication, and spectroscopy [1–4]. However, the THz range still remains a challenge for modern technology due to the lack of a compact, powerful, and scalable solid state source [5]. This problem is known as the *terahertz gap*.

To ‘close’ this gap from the lower frequencies, one can mention electronic devices with negative differential resistance (NDR). For instance, super-lattice electronic devices (SLED) generate higher harmonics by means of NDR [6] and can reach 0.5 THz gap, while the output power is less than 0.5 mW [7]. The radiation power of resonant tunneling diodes (RTDs) [8] is less than 1 μ W, and it further decreases by three orders of magnitude at room temperature. Also, RTDs suffer from their small electron transition times and parasitic capacitance, associated with the double-barrier structure.

The use of layered high-temperature superconductors (HTSC) with intrinsic Josephson junctions, such as BIS-CCO [9–11] can produce radiation with Josephson oscillations generated by an applied bias voltage [12, 13]. Here a tunable emission, from 1 to 11 THz, has been recently observed [14]. However, the power output is 1 μ W, which is still inadequate for practical applications.

It can be enhanced with the use of Bose-Einstein condensates [15, 16]. However, such approach requires a hybridization of several bands with different parity, making the output power small. Quantum cascade lasers (QCL) [17–19] can generate a high-frequency THz-radiation, while transistors [20–23], Gunn diodes [24], and frequency multipliers [25] are approaching the THz-gap from the low-frequency side. The latter covers the whole THz range while having small power. The general

fundamental obstacle of all these THz sources is the small emission rate (of the order of 10 ms). It can be increased with the Purcell effect when the THz source is placed in a cavity [26, 27], however, the quantum efficiency is still about 1%, and the manufacture of these devices is difficult.

Graphene and carbon nanotubes may serve as highly tunable sources and detectors of THz radiation [28–34], and even in THz lasers [35–40]. In the dual-gate graphene-channel field-effect transistor [41] embedded into a cavity resonator [42, 43], one observes spontaneous broadband light emission in the 0.1-7.6 THz range with the maximum radiation power of $\sim 10 \mu$ W at the temperature 100 K. There are also emerging sources of THz-radiation that can deliver several frequencies at room temperature, e.g., multiple harmonic generation in superlattices [44, 45], frequency difference generation in mid infrared QCLs [46] and THz optical combs [47].

Graphene covered with a thin film of colloidal quantum dots has strong photoelectric effect, that provides enormous gain for the photodetection (about 10^8 electrons per photon) [48]; graphene grown on SiC has strong photoresponse [49]; and graphene composites can improve solar cells efficiency [50]. Note, both graphene and superconductor alone are practically insensitive to light [51]. In this Letter, we show that graphene placed in the vicinity of a superconductor represents an active media with strong light-matter coupling. It can operate as an optical transistor that amplifies broadband electromagnetic radiation. This new feature allows one to use this device for studying chemical and biological processes or in telecommunications for encryption-decryption procedures, where it is important to image the whole spectrum.

We consider a system consisting of parallel layers of graphene and a superconductor, exposed to an electromagnetic (EM) field incident with the angle θ and linearly polarized along the x-z plane (p-polarisation), $\mathbf{E}(\mathbf{r}, t) = (\sin \theta, \mathbf{0}, \cos \theta) E_0 e^{-i(k_{\perp} z + \mathbf{k}_{\parallel} \cdot \mathbf{r} + \omega t)}$, where \mathbf{k}_{\parallel} ,

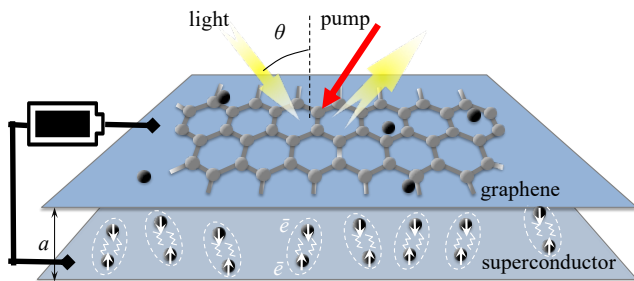


FIG. 1. System schematic. Graphene coupled with a two-dimensional superconductor by the Coulomb force and connected to an electrical pump source (a battery). Figure also shows the pump-probe configuration for the THz radiation amplification: The hybrid system is exposed to an external laser (*pump*, depicted by red arrow) and broadband EM field at incidence angle θ (*probe*, depicted by yellow arrows). The frequency of the pump (probe) should be above (below) the superconducting gap. Both the optical and electrical pump can provide energy for the amplification.

ω , and \mathbf{r} are the in-plane wave vector of the field, frequency, and coordinate, respectively (see Fig. 1). Between graphene layer and superconductor there is a gate voltage that controls its chemical potential and provides AC power. It may pump the energy in the superconductor with AC bias, larger than the superconducting gap exciting quasiparticles and creating NDR. Alternatively, the battery can be replaced by an external laser (pump) with frequency exceeding the superconducting gap (Fig. 1).

The electrons in graphene are coupled by the Coulomb interaction, which has the Fourier image given by $v_k = 2\pi e^2/k$, where \mathbf{k} is in-plane momentum (lying in the x - y plane). The electrons between the two layers are also Coulomb-coupled, and the Fourier image of the interlayer interaction reads $u_k = 2\pi e^2 \exp(-ak)/k$, where $a \sim 10$ nm is the separation between the layers.

Using the linear response theory for hybrid systems [52, 53], we can write the electron density fluctuations in the graphene layer $\delta n_{k\omega}$ and Cooper pair density fluctuations in the superconducting layer $\delta N_{k\omega}$ as [54]

$$\begin{aligned} \delta n_{k\omega} &= \Pi_{k\omega}(v_k \delta n_{k\omega} + u_k \delta N_{k\omega} + W_{k\omega}), \\ \delta N_{k\omega} &= P_{k\omega}(v_k \delta N_{k\omega} + u_k \delta n_{k\omega} + W_{k\omega}), \end{aligned} \quad (1)$$

where $\Pi_{k\omega} = \Pi_{k\omega}^R + i\Pi_{k\omega}^I$ and $P_{k\omega} = P_{k\omega}^R + iP_{k\omega}^I$ are the complex-valued polarization operators of the graphene and superconductor, respectively, and $W_{k\omega} = eE_0/ik$ is the Fourier image of the potential energy due to the external electric field. From Eqs. (1) we can find the density fluctuations in graphene $n_{k\omega}$ and in superconductor $N_{k\omega}$ as linear functions of applied electric field amplitude E_0 (see Supplemental Material [55] for details). Collective plasmonic hybrid modes in graphene and superconductor can be found from the same system of equations, taking into account the expressions for the polarization loops of

the superconductor [54] and graphene [56, 57]. Substituting the expressions for $n_{k\omega}$ and $N_{k\omega}$ into the continuity equations, $kj_{k\omega} = -e\omega\delta n_{k\omega}$ and $kJ_{k\omega} = -2e\omega\delta N_{k\omega}$, for graphene and superconductor, respectively, we can determine the electric currents in each of the layers and their impedances Z_G and Z_{SC} . The collective modes of the hybrid system are presented in Fig. 2(a) for the undoped and doped graphene cases. The upper mode has a gap $2\Delta = 2$ meV. If in this hybrid a single graphene layer is not interacting with a superconductor, only one mode exists, which is due to the superconductor.

The formula for the power absorption or gain reads [58]

$$P(\omega) = \frac{1}{2} \left\langle \mathcal{R}e \left[\int d^2r \mathbf{J}(\mathbf{r}, t) \cdot \mathbf{E}^*(\mathbf{r}, t) \right] \right\rangle, \quad (2)$$

where the integration is over the graphene plane, $\langle \dots \rangle$ denotes time-averaging. We normalize the power with the sample area $\int d^2 = l^2$ and the square of the field amplitude E_0^2 to get

$$P(\omega) = \frac{P(\omega)}{l^2 E_0^2} = \frac{1}{2} \frac{e\omega}{kE_0} \mathcal{R}e[\delta n_{k\omega}]. \quad (3)$$

Figure 2(b) shows the dependence of the power absorption on the EM field incidence angle θ calculated with (3), fixing $\mu = 0$ at the Dirac point by gate voltage. All the curves exhibit critical angles at which the power absorption becomes negative, $\alpha < 0$. This suggests that the incident angle can be used to switch the amplifier device on or off. Furthermore, increasing the frequency of the incident EM wave increases the critical angle.

Figure 2(c) shows the power absorption spectrum. We see that coupling graphene to the superconductor layer results in a negative power absorption in THz frequency range (solid curves and the shaded regions). There is no negative absorption region for isolated graphene, where the power absorption remains positive for any frequency ν (dashed curves). When the light incidence angle θ increases, both the maximal intensity (slightly) and the frequency range of the negative light absorption increase, see the shaded area in Fig. 2(b,c). Thus, the angle of light incidence allows us to control the range of light frequencies with the negative absorption.

To understand the θ -dependence, note that the wave vector of the plasma wave is related to the projection of the incident light wave vector on the plane of the sample. Both the angular dependence of the absorption and gain are related to the amplitude of this wave propagating on the surface. The light incident perpendicular to the graphene surface can not excite such plasma waves and therefore, in this case we do not have the gain. However, at large incident angle, there is a reflection of the incident radiation due to the difference in the refractive index of the hybrid and air. Thus we conclude that the most optimal effect will be observed at small but nonzero θ . If the system is embedded into a cavity resonator, there might

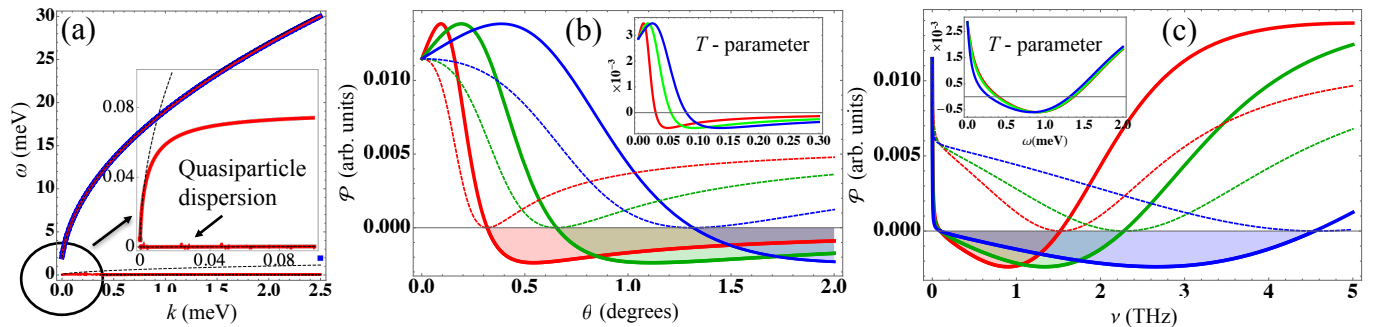


FIG. 2. (a) Hybrid collective plasmonic modes for undoped (blue curves) and doped (red curves, $\mu = 3.0$ meV) graphene layer. Black dashed curves show the modes of isolated doped graphene layer. Inset. zoom-in of the lower energy modes. (b) Power absorption as a function of the angle of incidence θ [see also Fig. 1] for graphene-superconductor hybrid for frequencies $\nu = 0.5$ THz (red), 1.0 THz (green), and 2.0 THz (blue). (c) Graphene power absorption spectrum for the angles of incidence $\theta = 1.0^\circ$ (red), $\theta = 1.5^\circ$ (green), and $\theta = 3.0^\circ$ (blue). Dashed curves show the data corresponding to the isolated graphene case. In (b) and (c) $\mu = 0$; in insets, the effect of temperature $T = 0$ (red), $T = 0.5T_c$ (green), and $T = T_c$ (blue) is shown. The separation between graphene and superconductor is $a = 10$ nm.

even arise lasing similar to one observed in plasmonic lattices [59, 60] or semiconductor superlattices [43].

The mechanism of gain here is similar to one in a waveguide coupled with a superconducting Josephson junction [61]. Then, the optical reflectivity of the system reads $\Gamma = (Z_G - Z_{SC})^2 / (Z_G + Z_{SC})^2$. Near the frequency of the plasmon resonance, there is an area of negative differential resistance of the superconductor, $R_{SC} < 0$. If we assume $X_G = 0$ and $X_{SC} = 0$ [61, 62], we find $\Gamma > 1$. Note, that graphene can also have NDR (see Sec. III of [55] and [63–65]) as in a graphene transistor, which consists of two graphene layers separated by a BN insulator [66].

The graphene-superconductor junction (Fig. 1) has large tunneling resistance. An electron in graphene with energy below the superconducting gap can tunnel into superconductor only due to the Andreev scattering [67]. The probability of such tunnelling is small since all electrons are paired. Therefore, the resistance of the junction is high. With applied bias voltage above the gap, quasiparticles appear and they can tunnel. As a result, the resistance decreases and NDR arises. The latter can appear even at zero bias when we pump the superconductor with external light with the frequency above the gap. The light excites electron and hole quasiparticles coexisting with superconducting fluctuations on the surface of the superconductor [68]. Then, in addition to the Andreev scattering, there starts normal tunneling of quasiparticles into the superconductor. The resistance of the junction decreases and the NDR arises. Such mechanism of NDR can exist only in a highly nonequilibrium excited state created by the pump.

Scattering and de-phasing mechanisms are limiting the gain bandwidth and can flat and eliminate the gain [69]. Here the plasmon scattering within each and between two graphene and superconducting layers can not only

broaden the width of the optical transition, but also enable optical gain and absorption to coexist, constituting the Wacker-Pereira mechanism of optical gain [69–71], as observed in QCLs [72, 73]. It provides one of the explanations, why $\alpha(\omega) = 1 - \Gamma(\omega)$ is negative below the plasmon resonance.

From another perspective, graphene separated by dielectric layer (e.g., made of BN, SiO₂ or Ta₂O₅) from the superconductor (Nb, Pb, or HTSC) together form a parallel plate capacitor, which capacitance C is given by $C = C_{plate} + C_q$, where C_{plate} is the classical capacitance $C_{plate} = \epsilon_0 A / a$, A is the area of the sample and ϵ_0 is the dielectric constant (e.g., $\epsilon_0 = 3.9$ for SiO₂). The quantum capacitance C_q of graphene emerges due to its conical energy-momentum relation, and it has the form $C_q = 2Ae^2 |E_F| / \pi \hbar^2 v_F^2$ [74–76].

This parallel plate capacitor is connected to a power supply that charges the capacitor and provides the energy for the amplification of incident radiation. The incident light (in particular, its component parallel to the superconducting surface) induces the fluctuation of charge density δn_s , which is associated with a travelling plasmon wave with the amplitude $E_s \sim \delta n_s$, where $\delta n_s = \delta n_{s0} \cos(kx + \omega t)$ (Fig. 3). This charge density wave on the surface of the superconductor generates a mirror charge wave of the opposite sign in the neutral graphene layer, being of the same order as the charge fluctuations in superconducting layer, i.e. $\delta n_G \sim \delta n_s$. Note that the sign of these charge density fluctuations changes each half-wavelength of the plasmon wave. These plasmons have the wavelength larger than a micrometer, and therefore the charge density for each half-wavelength can be viewed at as a local temporary graphene doping, moving with the wave. During this half-period, the charge fluctuation corresponds to the local change in the chemical potential or the Fermi energy E_F , which is directly

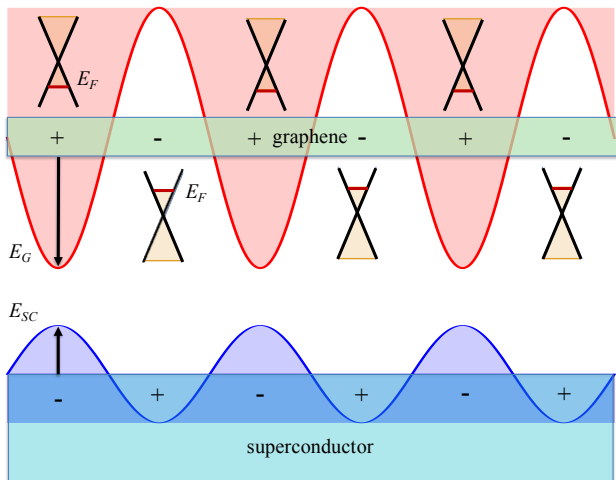


FIG. 3. Schematic of the mechanism of THz amplification. The incident light induces a collective hybrid plasmon mode. The interplay between this mode and the quantum capacitance of graphene amplifies the incident electromagnetic field (see text for details).

related to the amplitude of the plasmon wave propagating in graphene E_G . Due to the quantum capacitance of graphene, described by the relation $E_F \sim \sqrt{n_G}$, the waves amplitude, $E_G \sim E_F$, is significantly enhanced and it is different from the amplitude of the plasmon wave, propagating on the surface of the superconductor.

In order to stimulate radiation of electromagnetic waves in the THz range (similar to photo-conductive antennas [77]), one has to add a supply of energy. It can be done by introducing a pump-probe setup, where the energy required for the amplification of the probe comes from the pump. For the pump, we have to expose graphene to an external laser with the frequency above the superconducting gap. Or we can apply AC bias voltage with the amplitude larger than the gap. Due to pump, there forms a state, in which energy is accumulated in electronic excitations. To have the pump-probe configuration, we expose the junction to an additional external light (probe) with the frequency lower than the gap. Then, there on the surface will emerge superconducting charge density fluctuations. Effectively they represent coherent waves traveling inside the capacitor formed by graphene and superconductor. Due to the graphene quantum capacitance [74–76], the amplitude of these electromagnetic waves becomes amplified (by pump), resulting in reflection coefficient larger than 1 (as shown above).

Note that the graphene–superconductor system possesses many benefits. Both superconducting and graphene layers have giant mobility and small resistivity giving rise to minute losses. With increasing temperature the superconducting gap decreases, while graphene mobility changes a little. Since the radiation amplification

occurs in graphene the temperature has a weak effect on the operation of THz transistor (see insets in Fig. 2(b,c)). The working temperature range is similar to one for the stack of the Josephson junctions made of HTSC [9, 10] and it is limited by the critical temperature T_c .

The radiation power reads $P_r = \langle V_g I \rangle$, where the voltage V_g and the transverse current I are periodically changing in time around the Dirac point. Then, assuming simple periodic behavior for both $I(t)$ and $V_g(t)$ and the graphene-superconductor separation, $a=10$ nm [82], the maximal outcome power reads $\langle I \times V_g \rangle \sim 200\text{--}250 \mu\text{W}/\text{cm}^2$ [81]. Evidently, it can be increased for larger areas of the surface or employing multilayer hybrid structures.

Conclusions. We have shown that in a hybrid graphene–superconductor system exposed to an electromagnetic field of light the absorption coefficient can become negative in a certain range of frequencies and at a non-zero angle of incidence. We suggest that the system can serve as an amplifier of THz radiation. The essence of the amplification is the quantum capacitance of graphene, which provides the conversion of the charge density wave induced by incident light into emitted radiation with much stronger intensity. That is also related to the negative differential conductivity of the hybrid, where there is a strong Coulomb coupling of graphene and superconductor.

Such devices are now in strong demand and may be complementary to quantum cascade lasers. Moreover, the usage of high-temperature superconductors extends the range of temperatures required for their operation. The existence of Dirac or Weyl cones in graphene, topological insulators, and Weyl semimetals brings in a new physical concept called quantum capacitance. Its essence is in a strong dependence of the Fermi energy on the charge doping. A weak charge density wave can induce a strong electric field in these materials, allowing us to achieve the amplification of incident electromagnetic radiation.

The situation is somewhat similar to lasers, where the pumping results in the population inversion. The difference is that here the amplification can occur in a broad frequency range simultaneously, while in lasers it is pinned to a specific resonant frequency. Such amplification of the broadband spectrum, e.g., for chaotic or noise radiation, opens exciting opportunities of new types of molecular and biological noise spectroscopy, where the response of the system can be measured in a broad frequency range opening new opportunities in molecular and biological noise spectroscopy [83, 84].

Acknowledgements. We thank Vadim Kovalev and Gennadii Sergienko for fruitful discussions. K.H.V. and I.G.S. acknowledge the support of the Institute for Basic Science in Korea (Project No. IBS-R024-D1) and the grant RFBR 18-29-20033 mk. The work of F.V.K. was supported by the Government of the Russian Federation

through the ITMO Fellowship and Professorship Program.

* Corresponding author: F.Kusmartsev@lboro.ac.uk

- [1] F. H. Raab, P. Asbeck, S. Cripps, P. B. Kenington, Z. B. Popovic, N. Potheary, J. F. Sevic, and N. O. Sokal, Power amplifiers and transmitters for RF and microwave. *IEEE transactions on Microwave Theory and Techniques*, **50**(3), 814 (2002).
- [2] J. M. Chamberlain, Where optics meets electronics: recent progress in decreasing the terahertz gap. *Philosophical Transactions of the Royal Society of London A: Mathematical, Physical and Engineering Sciences* **362**(1815), 199, (2004).
- [3] H. Eisele, State of the art and future of electronic sources at terahertz frequencies. *Electronics letters*, **46**(26), 8, (2010).
- [4] D. M. Mittleman, Twenty years of terahertz imaging, *Optics express*, **26**(8), 9417, (2018).
- [5] D. Dragoman and M. Dragoman, Terahertz fields and applications, *Prog. Quantum Electron.* **28**(1), 1-66, (2004).
- [6] K. N. Alekseev, E. H. Cannon, F. V. Kusmartsev, and D. K. Campbell, Fractional and unquantized dc voltage generation in THz-driven semiconductor superlattices, *Europhys. Lett.* **56**(6), 842 (2001).
- [7] H. Eisele, L. Li, and E. H. Linfield, High-performance GaAs/AlAs superlattice electronic devices in oscillators at frequencies 100-320 GHz, *App. Phys. Lett.* **17** 172103 (2018).
- [8] T. Maekawa, H. Kanaya, S. Suzuki, and M. Asada, Oscillation up to 1.92 THz in resonant tunneling diode by reduced conduction loss, *Appl. Phys. Expr.* **9**(2), 024101 (2016).
- [9] L. Ozyuzer, A. E. Koshelev, C. Kurter, N. Gopalsami, Q. Li, M. Tachiki, K. Kadowaki, T. Yamamoto, H. Minami, H. Yamaguchi, and T. Tachiki, Emission of coherent THz radiation from superconductors, *Science* **318**(5854), 1291 (2007).
- [10] U. Welp, K. Kadowaki, and R. Kleiner, Superconducting emitters of THz radiation, *Nature Photonics* **7**(9), 702 (2013).
- [11] S. Hancong, et al., Compact High-T_c Superconducting Terahertz emitter operating up to 86 K, *Physical Review Applied*, **10**(2), 024041 (2018).
- [12] M. Gaifullin, et al., Collective Josephson plasma resonance in BiSCCO. *Phys. Rev. Lett.*, **75**(24), 4512 (1995).
- [13] M. Gaifullin et al., Abrupt change of Josephson plasma frequency in BiSCCO. *Phys. Rev. Lett.*, **84**(13), 2945 (2000).
- [14] E. A. Borodianskyi and V. M. Krasnov, Josephson emission with frequency span 1-11 THz from small Bi₂Sr₂CaCu₂O₈ mesa structures, *Nat. Commun.* **8**, 1742, (2017).
- [15] K. V. Kavokin, M. A. Kaliteevski, R. A. Abram, A. V. Kavokin, and S. Sharkova, Stimulated emission of terahertz radiation by exciton-polariton lasers, *Appl. Phys. Lett.* **97**, 201111 (2010).
- [16] I. G. Savenko, I. A. Shelykh, and M. A. Kaliteevski, Non-linear terahertz emission in semiconductor microcavities, *Phys. Rev. Lett.* **107**, 027401 (2011).
- [17] R. Köhler, A. Tredicucci, F. Beltram, H. E. Beere, E. H. Linfield, A. G. Davies, D. A. Ritchie, R. C. Iotti, and F. Rossi, Terahertz semiconductor-heterostructure laser, *Nature* **417**, 156 (2002).
- [18] B. S. Williams, Terahertz quantum-cascade lasers, *Nat. Photon.* **1**, 517 (2007).
- [19] J. Faist, *Quantum cascade lasers*, OUP Oxford (2013).
- [20] H. W. Hübers, S. G. Pavlov, and V. N. Shastin, Terahertz lasers based on germanium and silicon, *Semicond. Sci. Technol.* **20**, S211 (2005).
- [21] Y. Chassagneux, R. Colombelli, W. Maineult, S. Barbieri, H. E. Beere, D. A. Ritchie, S. P. Khanna, E. H. Linfield, and A. G. Davies, Electrically pumped photonic-crystal terahertz lasers controlled by boundary conditions, *Nature* **457**, 174 (2009).
- [22] J. Lusakowski, W. Knap, N. Dyakonova, L. Varani, J. Mateos, T. Gonzalez, Y. Roelens, S. Bollaert, A. Cappy, K. Karpietz, Voltage tuneable terahertz emission from a ballistic nanometer InGaAs/InAlAs transistor, *J. Appl. Phys.* **97**, 064307 (2005).
- [23] P. Li, Y. C. Wang, and J. Z. Zhang, All-optical fast random number generator, *Opt Express*. **18**, 20360 (2010).
- [24] S. Pérez, T. González, D. Pardo, and J. Mateos, Terahertz Gunn-like oscillations in InGaAs/InAlAs planar diodes *J. Appl. Phys.* **103**, 094516 (2008).
- [25] A. Maestrini, J. S. Ward, J. J. Gill, C. Lee, B. Thomas, R. h. Lin, G. Chattopadhyay, and I. Mehdi, A frequency-multiplied source with more than 1 mW of power across the 840-900-GHz band, *IEEE Trans. Microwave Theory Technol.* **58**, 1925 (2010).
- [26] Y. Todorov, I. Sagnes, and I. Abram, and C. Minot, Purcell Enhancement of Spontaneous Emission from Quantum Cascades inside Mirror-Grating Metal Cavities at THz Frequencies, *Phys. Rev. Lett.* **99**, 223603 (2007).
- [27] Y. Chassagneux, R. Colombelli, W. Maineult, S. Barbieri, H. E. Beere, D. A. Ritchie, S. P. Khanna, E. H. Linfield and A. G. Davies, Electrically pumped photonic-crystal terahertz lasers controlled by boundary conditions, *Nature (London)* **457**, 174 (2009).
- [28] M. E. Portnoi, O. V. Kibis, and M. Rosenau da Costa, *Proc. SPIE* **6328**, 632805 (2006).
- [29] O. V. Kibis, M. Rosenau da Costa, and M. E. Portnoi, Generation of terahertz radiation by hot electrons in carbon nanotubes, *Nano letters* **7**(11) 3414 (2007).
- [30] M. E. Portnoi, O. V. Kibis, and M. Rosenau Da Costa, Terahertz applications of carbon nanotubes, Superlattices and Microstructures **43**(5-6) 399 (2008).
- [31] S. A. Mikhailov, *Microelectron. J.* **40**, 7125 (2009).
- [32] K. G. Batrakov, O. V. Kibis, P. P. Kuzhir, M. Rosenau Da Costa, and M. E. Portnoi, Terahertz processes in carbon nanotubes, *Journal of Nanophotonics* **4**(1) 041665 (2010).
- [33] R. Hartmann, J. Kono, and M. E. Portnoi, Terahertz science and technology of carbon nanomaterials, *Nanotechnology* **25**, 322001 (2014).
- [34] V. Ryzhii, T. Otsuji, M. Ryzhii, et al., Graphene vertical cascade interband terahertz and infrared photodetectors, *2D Mater* **2** 25002 (2015).
- [35] D. Yadav, S. B. Tombet, T. Watanabe, S. Arnold, V. Ryzhii, T. Otsuji, Terahertz wave generation and detection in double-graphene layered van der Waals heterostructures, *2D Mater* **3**, 45009 (2016).
- [36] A. Satou, T. Otsuji, V. Ryzhii, Theoretical study of population inversion in graphene under pulse excitation, *Jpn*

- J Appl. Phys **50**, 70116 (2011).
- [37] A. Satou, V. Ryzhii, Y. Kurita, T. Otsuji, Threshold of terahertz population inversion and negative dynamic conductivity in graphene under pulse photoexcitation. J Appl Phys **113** 143108 (2012). V. Ryzhii, M. Ryzhii, V. Mitin, A. Satou, T. Otsuji, Effect of heating and cooling of photogenerated electron-hole plasma in optically pumped graphene on population inversion, Jpn J Appl Phys **50**, 094001 (2011).
- [38] T. Otsuji, S. B. Tombet, A. Satou, M. Ryzhii, V. Ryzhii, Terahertz-wave generation using graphene: toward new types of terahertz lasers, IEEE J Sel Top Quantum Electron **19**, 8400209 (2013).
- [39] S. Boubanga-Tombet, S. Chan, T. Watanabe, A. Satou, V. Ryzhii, T. Otsuji, Ultrafast carrier dynamics and terahertz emission in optically pumped graphene at room temperature, Phys Rev B **85** 35443 (2012).
- [40] T. Li, L. Luo, M. Hupalo, et al., Femtosecond population inversion and stimulated emission of dense dirac fermions in graphene, Phys Rev Lett **108** 167401 (2012).
- [41] V. Ryzhii, M. Ryzhii, V. Mitin, T. Otsuji, Toward the creation of terahertz graphene injection laser. J Appl Phys. **110**, 094503;
- [42] Y. Deepika, G. Tamamushi, T. Watanabe, et al., Terahertz light-emitting graphene-channel transistor toward single-mode lasing, Nanophotonics, **7**(4), 741 (2018).
- [43] A. E. Hramov, V. V. Makarov, A. A. Koronovskii, F. V. Kusmartsev, et al., Subterahertz chaos generation by coupling a superlattice to a linear resonator, Phys. Rev. Lett. **112**, 116603 (2014).
- [44] M.F. Pereira et al , Physical Review B 96 (4), 045306 (2017).
- [45] A. Apostolakis and M. F. Pereira, AIP Advances 9, 015022 (2019).
- [46] M. Razeghi et al, Optics Express 23, 8462 (2015);
- [47] THz optical combs A. Forrer et al, Optics Express 26, 23167 (2018).
- [48] G. Konstantatos, M. Badioli and F. H. L. Koppens, Hybrid graphene-quantum dot phototransistors with ultrahigh gain, Nature Nanotechnology, **7**, 363-368 (2012).
- [49] A. B. G. Trabelsi, F. V. Kusmartsev, M. B. Gaifullin, A. Kusmartseva, M. Oueslati, Morphological imperfections of epitaxial graphene: from a hindrance to the generation of new photo-responses in the visible domain, Nanoscale **9**, 11463-11474 (2017).
- [50] R. Bkatri, O. E. Kusmartseva, F. V. Kusmartsev, et al., Degree of phase separation effects on the charge transfer properties of P3HT: Graphene nanocomposites, J. of Luminescence **161**, 264-270 (2015).
- [51] K. C. Yung, W. M. Wu, M. P. Pierpoint, F. V. Kusmartsev, Introduction to graphene electronics – a new era of digital transistors and devices, Contemporary Physics **54**, 233-251 (2013).
- [52] M. V. Boev, V. M. Kovalev, I. G. Savenko, Magnetoplasmon Fano resonance in Bose-Fermi mixtures, Phys. Rev. B **94**, 241408(R) (2016).
- [53] V. M. Kovalev and I. G. Savenko, Paramagnetic resonance in spin-polarized disordered Bose-Einstein condensates, Sci. Rep. **7** (1), 2076 (2017).
- [54] K. H. A. Villegas, V. M. Kovalev, F. V. Kusmartsev, and I. G. Savenko, Shedding light on topological superconductors, Phys. Rev. B **98**, 064502 (2018).
- [55] See Supplemental Material [URL] for the details of derivations.
- [56] B. Wunsch, T. Stauber, F. Sols, and F. Guinea, Dynamical polarization of graphene at finite doping, New J. Phys. **8**, 318 (2006).
- [57] E. H. Hwang and S. Das Sarma, Dielectric function, screening, and plasmons in two-dimensional graphene, Phys. Rev. B **75**, 205418 (2007).
- [58] L. D. Landau and E. M. Lifshitz, Electrodynamics of continuous media, Pergamon press (1960).
- [59] Plasmons can be treated as bosons obeying the Bose-Einstein distribution. However under external irradiation there can appear a virtual inversion of their population and their continuous stimulated emission (positive gain) accompanied by the amplification of the incident light. In our case, it corresponds to $\alpha < 0$.
- [60] W. Zhou, M. Dridi, J. Y. Suh, C. H. Kim, D. T. Co, M. R. Wasielewski, G. C. Schatz, and T. W. Odom, Nature Nanotechnol. **8**, 506 (2013).
- [61] N. F. Pedersen and S. Madsen, THz generation using fluxon dynamics in high temperature superconductors, IEEE Transactions on Applied Superconductivity **19**, 726-729 (2009).
- [62] Note, that here the absorption and gain have been calculated directly as the power of the absorbed or emitted electromagnetic radiation with Eq. (8), on the basis of the solutions of Eqs. (1-6) . The concept of impedance has not been used in this calculation. However, from the same equations, one can find impedances of graphene and SC as coefficients proportional to density fluctuations of graphene and superconductor, or AC electric currents expressed through these density variations, respectively, over E_0 . After changing of variables, Eqs. (1)-(3) can be presented in the form, where these impedances are unknown variables. Then the results obtained for the gain by direct calculation of the emitted power can be interpreted with the concept of the graphene and superconductor impedances, characterising the hybrid system. This argument with impedances for graphene and SC has been used just for clarification of the effect and it provides an alternative interpretation of the gain phenomenon.
- [63] R. Kummel, U. Günsenheimer, and R. Nicosky, Andreev scattering of quasiparticle wave packets and current-voltage characteristics of superconducting metallic weak links, Phys. Rev. B, **42**(7), 3992,(1990).
- [64] T. Hyart, K. N. Alekseev, and E. V. Thuneberg, Bloch gain in dc-ac-driven semiconductor superlattices in the absence of electric domains, Phys. Rev. B **77**(16) 165330 (2008).
- [65] T. Hyart, M. Jussi, and K. N. Alekseev, Model of the influence of an external magnetic field on the gain of terahertz radiation from semiconductor superlattices, Phys. Rev. Lett. **103**, 117401 (2009).
- [66] L. Britnell, R. V. Gorbachev, A. K. Geim, L. A. Ponomarenko, A. Mishchenko, M. T. Greenaway, T. M. Fromhold, K. S. Novoselov, and L. Eaves, Resonant tunnelling and negative differential conductance in graphene transistors, Nature Comm. **4**, 1794 (2013).
- [67] A. Andreev, Sov. Phys. JETP **19**, 1228 (1964).
- [68] L. Aslamazov and A. Larkin, Sov. Phys. Solid State **10**, 875 (1968).
- [69] M.F. Pereira Jr and S. Tomić, Appl. Phys. Lett., **98**(6), 061101 (2011).
- [70] A. Wacker, Quantum cascade laser: An emerging technology, Nonlinear Laser Dynamics, Berlin (2012).

- [71] A. Wacker, Lasers: Coexistence of gain and absorption, *Nature Phys.*, **3**, 298-299 (2007).
- [72] R. Terazzi, T. Gresch, M. Giovannini, N. Hoyler, N. Sekine, and J. Faist, Bloch gain in quantum cascade lasers, *Nature Phys.*, **3**(5) 329 (2007).
- [73] D. G. Revin, M. R. Soulby, J. W. Cockburn, Q. Yang, C. Manz, and J. Wagner, Dispersive gain and loss in midinfrared quantum cascade laser, *Appl. Phys. Lett.* **92**, 081110 (2008).
- [74] G. L. Yu et al. Interaction phenomena in graphene seen through quantum capacitance, *PNAS* **110**, 3282 (2013).
- [75] A. B. G. Trabelsi, F. V. Kusmartsev, B. J. Robinson, A. Ouerghi, O. E. Kusmartseva, O. V. Kolosov, R. Mazzocco, M. B. Gaifullin, and M. Oueslati, Charged nanodomains and bubbles in epitaxial graphene, *Nanotechnology*, **25**(16), 165704 (2014).
- [76] A. B. G. Trabelsi, F. V. Kusmartsev, D. M. Forrester, O. E. Kusmartseva, M. B. Gaifullin, P. Cropper, and M. Oueslati, The emergence of quantum capacitance in epitaxial graphene, *J. Mat. Chemistry C*, **4**(24), 5829 (2016).
- [77] Burford, N.M. and El-Shenawee, M.O., Review of terahertz photoconductive antenna technology. *Optical Engineering*, **56**(1), p.010901 (2017).
- [78] Note, that supporting zero chemical potential we expect to see a nonzero radiation power, which is just an average $V_g(t) \times I(t)$ over photocurrent period. The output power is maximised when the chemical potential is pinned at the Dirac point, since in this case the voltage variation $V_g(t)$ has a maximal amplitude. On the other hand, if we apply an external AC voltage $V_g(t)$ to the hybrid system, the transistor might radiate THz radiation even without external incident light. In this case, the radiation power of the system will be exactly proportional to $P = \langle V_g(t)I(t) \rangle$, where the average is taken over the oscillation period and here a fraction of this energy will be wasted in thermal Joule losses. However, such a source of THz radiation requires a special set up for the applied voltage to maximize the effect of quantum capacitance.
- [79] M. M. Glazov and S. D. Ganichev, High frequency electric field induced nonlinear effects in graphene, *Physics Reports* **535**, 101 (2014).
- [80] S. D. Ganichev and W. Prettl, *Intense Terahertz Excitation of Semiconductors*, Oxford University Press (2006).
- [81] Such time-dependent periodically-changing voltage $V_g(t)$ on graphene is associated with the plasma wave induced in graphene by the incident light. On average, the voltage variation vanishes, $\langle V_g \rangle = 0$, while the radiated power is not since the current has the same periodic oscillations and the power depends on their product [78]. During the operation of the device the voltage in graphene can reach 40-50 mV. That limit arises due to electron scattering by optical phonons, which will be generated at higher voltage with account for nonlinear effects [79, 80]. The driving photocurrent through 1 cm^2 of graphene is of the order of 10 mA, which value is limited by the Joule heating of the superconductor surface region.
- [82] In our calculations we used a relatively large value for the graphene-superconductor separation, $a=10 \text{ nm}$, which is several orders of magnitude smaller than the wavelength of THz radiation. The smaller the separation the stronger the effect. However, at very small separation there may arise a proximity effect. That limits the separation distance to a superconducting coherence length, which is for HTSC about $\sim 1-2 \text{ nm}$.
- [83] V. P. Koshelets et al., *IEEE Trans. Terahertz Sci. Technol.* **5**, 687 (2015).
- [84] D.R. Gulevich, V. P. Koshelets, and F. V. Kusmartsev, Josephson flux-flow oscillator: The microscopic tunneling approach. *Phys. Rev. B*, **96**(2), 024515 (2017).